JACS
JOURNAL OF THE AMERICAN CHEMICAL SOCIETY

Communication

pubs.acs.org/JACS

Ultralow Parasitic Energy for Postcombustion CO_2 Capture Realized in a Nickel Isonicotinate Metal–Organic Framework with Excellent Moisture Stability

Shyamapada Nandi,[†,⊥] Sean Collins,[§,⊥] Debanjan Chakraborty,[†] Debasis Banerjee,[∥] Praveen K. Thallapally,[*,∥] Tom K. Woo,[*,§] and Ramanathan Vaidhyanathan[*,†,‡]

[†]Department of Chemistry and [‡]Centre for Energy Science, Indian Institute of Science Education and Research, Pune 411008, India

[§]Centre for Catalysis Research and Innovation & Department of Chemistry and Biomolecular Sciences, University of Ottawa, Ottawa, Ontario K1N 6N5, Canada

[∥]Physical and Computational Science Directorate, Pacific Northwest National Laboratory, Richland, Washington 99354, United States

Supporting Information

ABSTRACT: Metal–organic frameworks (MOFs) have attracted significant attention as solid sorbents in gas separation processes for low-energy postcombustion CO_2 capture. The parasitic energy (PE) has been put forward as a holistic parameter that measures how energy efficient (and therefore cost-effective) the CO_2 capture process will be using the material. In this work, we present a nickel isonicotinate based ultramicroporous MOF, **1** [Ni-(4PyC)$_2$·DMF], that has the lowest PE for postcombustion CO_2 capture reported to date. We calculate a PE of 655 kJ/kg CO_2, which is lower than that of the best performing material previously reported, Mg-MOF-74. Further, **1** exhibits exceptional hydrolytic stability with the CO_2 adsorption isotherm being unchanged following 7 days of steam-treatment (>85% RH) or 6 months of exposure to the atmosphere. The diffusion coefficient of CO_2 in **1** is also 2 orders of magnitude higher than in zeolites currently used in industrial scrubbers. Breakthrough experiments show that **1** only loses 7% of its maximum CO_2 capacity under humid conditions.

Electrical power generation from fossil fuels, such as coal, accounts for about 40% of the world's anthropogenic CO_2 emissions.[1] Scrubbing the CO_2 from these stationary sources is seen as a practical means of meaningfully reducing emissions in the near term because existing power plants can be retrofitted with postcombustion CO_2 capture systems. Although large scale CO_2 scrubbers based on aqueous amines exist, they are not energy efficient enough to enable widespread carbon capture and have been estimated to increase the electricity costs by 60–80%.[2,3] These high energetic and associated monetary costs are the most significant technological challenges to large scale deployment of carbon capture and storage. Pressure and temperature swing adsorption (P/TSA) gas separation systems are considered among the most promising technologies to enable cost-effective postcombustion CO_2 capture[4] where CO_2 must be separated from a humid flue gas composed of ∼85% N_2,10–15% CO_2. In such systems, the combustion gas is passed through a solid sorbent bed, which selectively adsorbs CO_2. When the bed reaches capacity, the captured CO_2 is desorbed, releasing near pure CO_2 for storage. Zeolites, such as 13X, are currently used in large scale PSA systems for CO_2 scrubbing of natural gas and landfill gases.[5] Unfortunately, zeolites do not perform well in the humid gas streams of postcombustion CO_2 capture.[6] For this purpose, metal–organic frameworks (MOFs) have attracted significant attention due to their high functional tunability.[7,8]

Although MOFs with large CO_2 uptake capacities are often promoted as ideal materials for postcombustion CO_2 capture,[9] other adsorption properties are more important for low cost capture. In particular, the CO_2/N_2 selectivity, the CO_2 working capacity (the difference between the uptake capacity at the adsorption and desorption conditions) and heat of adsorption (HOA) are critical. Other physiochemical properties such as the thermal and hydrolytic stability are also critical.[10] To assess how energy efficient the CO_2 capture will be with a particular material, Smit and others have advocated using the parasitic energy (PE) as a single figure-of-merit to compare materials.[3] This is the energy required to regenerate the sorbent during the desorption process in addition to the subsequent energy cost to pressurize the CO_2 to 150 bar for transportation. The PE gives a pragmatic quantification of the efficiency of the solid sorbent used in these large scale separations. Recently, Huck et al.[3a] compared the PEs of MOFs and other solid sorbents such as zeolites. Mg-MOF-74 was found to have the lowest PE (727 kJ/kg of CO_2) of all materials evaluated. For comparison, the PEs for state-of-the-art aqueous amine technologies are estimated to be at least 1000 kJ/kg of CO_2.[3b,c] Although Mg-MOF-74 possesses a record low PE, it is known to irreversibly decompose in humid gas streams. One material that was computed to have a relatively low PE[3a] with significant moisture stability is the ultramicroporous SIFSIX-3-Zn.[11]

Herein we present a nickel isonicotinate based ultramicroporous MOF [Ni-(4Pyc)$_2$·DMF], **1** (IISERP-MOF**2**), with the lowest PE for postcombustion CO_2 capture reported to date. **1**'s CO_2 adsorption properties that are essentially

Received: October 7, 2016
Published: January 20, 2017

DOI: 10.1021/jacs.6b10455
J. Am. Chem. Soc. 2017, 139, 1734–1737

unchanged following steam-treatment and long exposure to humidity. **1** exhibits high CO_2 diffusion coefficient for favorable adsorption/desorption kinetics. Furthermore, breakthrough measurements on **1** under both dry and 50% RH conditions show that **1** retains most of its performance.

IISERP-MOF**2**,**1**, has a framework formed by linking isolated Ni octahedra by 4-pyridylcarboxylate ligands (Figure 1a). Each

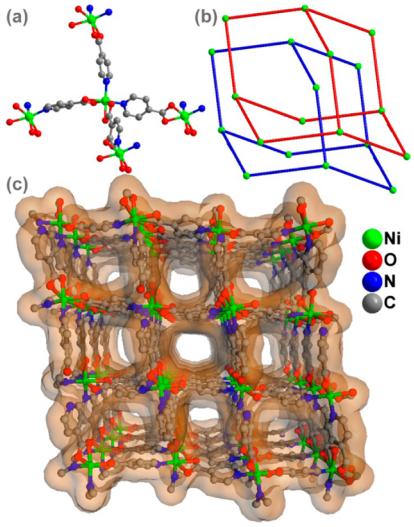

Figure 1. (a) Building unit of **1**, showing the coordination around the Ni center. (b) 2-fold interpenetrated diamondoid structure of **1** with only the Ni (green spheres) centers shown. (c) Connolly surface representation of **1** (probe radius = 1.4 Å) showing the ultramicroporous 1-D channels.

Ni octahedra is coordinated by bidentate carboxylate groups and two pyridyl units. Reducing the Pyc to linear linkers, the effective coordination around each Ni is tetrahedral and these nodes connect to form a classic adamantane unit of the diamondoid framework with a 2-fold interpenetration (Figure 1b and S2). The interpenetration blocks most channels of the individual framework leaving only square shaped, 7 × 7 Å channels (excluding van der Waals radii) along the *a*-axis as shown in Figure 1c. Using a DFT model the pore size (C, CO_2 @ 273 K) for **1** was estimated to be 4.7 Å. **1** is compositionally related to an ultramicroporous nickel isonicotinate MOF, **2**, $(Ni_9(\mu\text{-}H_2O)_4(H_2O)_2(C_6NH_4O_2)_{18})$, that has been reported elsewhere.[10a] **2** is built from similar SBU's as **1**, but is non-interpenetrated.

N_2 isotherms of **1** at 77, 273, and 303 K are shown in Figure 2a. A BET surface area of 470 m^2/g and a Langmuir surface area of 700 m^2/g have been determined for **1**. A surface area of 505 m^2/g is calculated using the crystal structure and a N_2 probe. Figure 2b shows the CO_2 adsorption isotherms of **1** at 195, 303, 313, and 333 K. Interestingly, at 195 K the material uptakes ~7 mmol/g of CO_2 which is nearly the same as the saturation uptake it has for N_2 (cf. 77 K N_2 isotherm). This suggests that both gases are able to see the same accessible pores at low temperature. At 303 K and 0.15 bar, the CO_2 uptake of **1** is 1.6 mmol/g. The HOA for CO_2 in **1** was determined to be moderate (33 kJ/mol) via both virial fits and a DFT model (Supporting Information). **1** shows a fairly consistent HOA across all loadings (Figure 2c and S18). Grand-canonical Monte Carlo simulations were performed to examine the CO_2–framework interactions. Four unique CO_2 binding sites were identified (see Supporting Information).

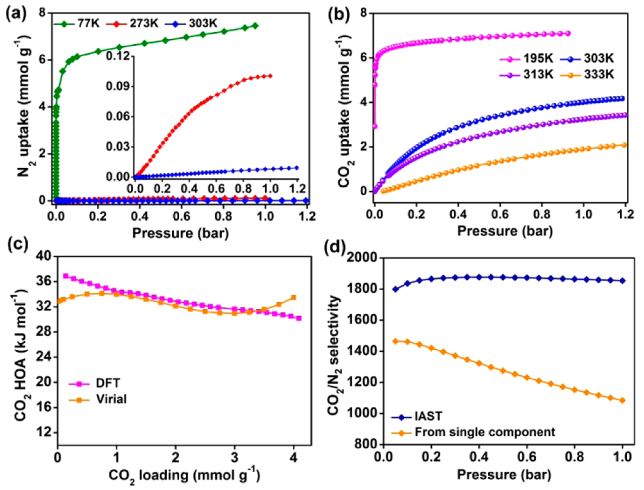

Figure 2. (a) N_2 adsorption isotherms of **1**. Inset: zoom-in of the isotherms at 273 and 313 K. (b) CO_2 adsorption isotherms of **1**. (c) HOA plots for CO_2 in **1**. (d) CO_2/N_2 selectivity of **1** calculated at 313 K (composition: $14CO_2$:$86N_2$) using IAST and without considering competitive binding.

Analysis of the CO_2–framework interactions in these binding sites reveals that the CO_2 molecules are primarily held by dispersion interactions with electrostatic interactions contributing less than 5% of the total binding energy in three of the four binding sites and 12% in the fourth site.

1 was found to adsorb unusually low amounts of N_2 at room temperature or higher, giving rise to exceptional CO_2/N_2 selectivities. Figure 2d shows the CO_2/N_2 selectivity of **1** calculated using the experimental single component isotherms and ideal adsorbed solution theory (IAST) with a composition of $14CO_2$:$86N_2$. At 1 bar and 313 K, conditions of relevance to postcombustion CO_2 capture, **1** has an exceptional CO_2/N_2 selectivity of 1853. We note that this high selectivity is not an artifact of the competitive binding model used as simply using adsorption values from the single component isotherms gives a value of 1084. The selectivity computed for **1** compares very favorably to other MOFs promoted for postcombustion CO_2 capture, such as Mg-MOF-74 (148 at 1 bar and 323 K with 0.15 bar CO_2 and 0.75 bar N_2)[9a] and SIFSIX-3-Zn (1818 at 1 bar and 298 K with 0.10 bar CO_2 and 0.9 bar N_2).[11a]

To compare the postcombustion CO_2 capture performance of **1** to other materials, the PEs were calculated following the methodology of Huck et al.[3a] Although in their work proprietary software was used to evaluate the compression terms of the PE, we used standard equations (Supporting Information). Nonetheless, comparing the PEs for 43 materials, our calculated results differed by only 4.5% on average compared to those reported by Huck with a Spearman rank correlation coefficient of 0.998. Figure 3 compares the PE calculated for **1** and a range of other reported materials where the total energy is broken down into the compression and thermal components. The PE for **1** was calculated to be 655 kJ/kg CO_2, lower than all materials.[3a] Interestingly, although **1** has the lowest reported PE of all materials, it is not the highest performing material in any one category. For example, materials such as Mg-MOF-74 have better CO_2 uptake and working capacities and SIFSIX-3-Cu has a higher CO_2/N_2 selectivity (5463) (Table S4). The HOA of **1** is not particularly low at 33 kJ/mol. For example, both UMCM-1 and MOF-177 have CO_2 HOAs of 10.9 and 13.7 kJ/mol, respectively. However, they

DOI: 10.1021/jacs.6b10455
J. Am. Chem. Soc. 2017, 139, 1734–1737

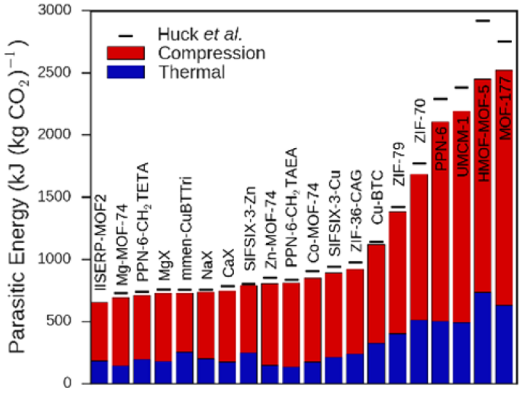

Figure 3. Optimized PEs (divided into thermal and compression components) of selected materials calculated with data taken from Huck et al.[3a] compared to that of **1**. For comparison, values calculated by Huck et al. are shown as black lines.

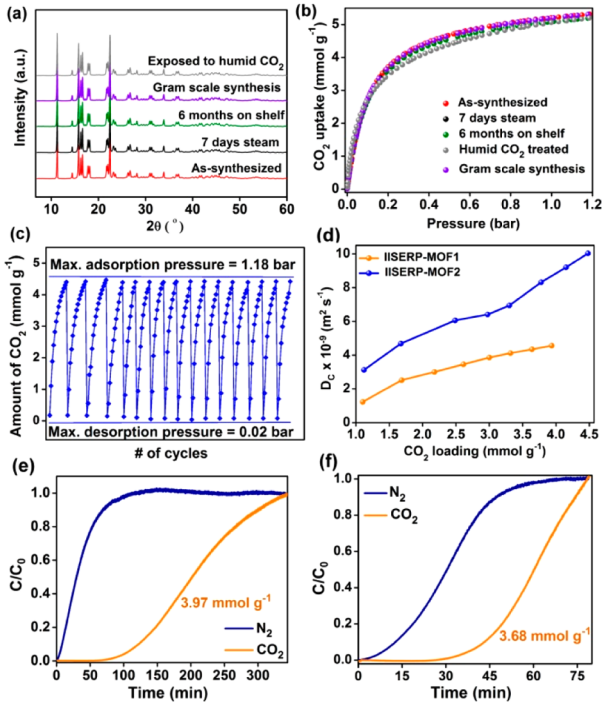

Figure 4. (a) PXRD pattern and (b) comparison of CO_2 adsorption isotherms of **1** to show moisture stability and scalability. (c) CO_2 adsorption−desorption cycles at 30 °C. (d) CO_2 self-diffusion coefficients from kinetics measurement. Values for IISERP-MOF**1** is taken from ref 10. Breakthrough measurements under (e) Dry and (f) 50% RH conditions. The amount of sample used in wet measurement was ∼1/3 of what was used in the dry measurements.

also possess very high PEs of greater than 2100 kJ/kg CO_2. One reason why **1** has such a low PE, is that it optimized to a high desorption pressure of 0.2 bar, while most materials achieved their minimum PE at desorption pressures of between 0.1 to 0.01 bar. The mild desorption pressure for **1** can, in part, be attributed to the strong response it has to the temperature increase from the adsorption to desorption conditions. It was found that the temperature increase from 313 to 333 K resulted in a 75% decrease in CO_2 adsorption at 0.15 bar. The high desorption pressure in **1** gives it the lowest energy of compression of all materials surveyed. If the energy required to place the system under vacuum is included in the total PE, **1** not only remains the best material in this respect but the difference in the PE to the next closest material increases from 39 to 86 kJ/kg CO_2 (Figure S33).

Aside from having a record low PE for postcombustion CO_2 capture, **1**, possesses other favorable characteristics for postcombustion CO_2 capture. Unlike Mg-MOF-74, which has open metal sites and is known to decompose in humid conditions,[12] **1** has no open metal sites and has exceptional hydrolytic stability. For example, following 7 days of steam-treatment at >85% RH, there was no loss of crystallinity or porosity in **1** as confirmed by the PXRD patterns and CO_2 sorption measurements (Figure 4a,b). The adsorption capacity at 0.15 bar CO_2 saw a decrease of only 1.7%. For the same sample that sat on the shelf for 6 months (exposed to the atmosphere with RH > 65%), the adsorption capacity dropped by only 2.4%. **1** withstands carbonic acid, which is known to form in humid CO_2 streams. The CO_2 adsorption isotherm of **1** remains unchanged following exposure to a flow of humid CO_2 for 24 h (see Supporting Information). CO_2 on/off cycling experiment was carried out on the ASAP2020HD adsorption instrument. During this, the sample was subjected to a pressure swing from 1.18 to 0.02 bar with each the sorption−desorption cycle lasting for 40 min. As can be seen from Figure 4c, the amount of CO_2 adsorbed remains constant and the cycling happens smoothly. This parallels the large diffusion coefficients (D_c) for CO_2 within the pores of the MOF (Figure 4d). The average D_c of **1** over a range of CO_2 loadings was found to be 6.04×10^{-9} m^2 s^{-1}, which is higher than that found in other MOFs with much larger pores such as MOF-5 (1.17×10^{-9} m^2 s^{-1}) or MOF-177 (1.17×10^{-9} m^2 s^{-1}).[13] Most notably, the D_c is more than 2 orders of magnitude higher than zeolite 13X, the currently used commercial PSA sorbent,[14] suggesting that ultramicroporous MOFs can be well-suited for gas separations.

To examine the adsorption kinetics in more real world conditions, breakthrough experiments were performed on **1** under dry and wet (50% RH) conditions (Figure 4e,f). In both cases, the N_2 comes off before the CO_2. Importantly, even under 50% RH **1** loses only about 7% of its maximum CO_2 capacity. This compares closely to what was observed for the SIFSIX-2-Cu-i.[11a] The CO_2 capacity of **1** under dynamic conditions was found to be 3.97 mmol/g, which is lower than NiMOF-74 (4.5 mmol/g) but higher than the members of SIFSIX series[15] and the FJU series,[16] whose breakthrough studies were carried out under a relatively higher flow rate (5 mL/min, see Supporting Information).

Few serious green house gas mitigation strategies do not include carbon capture and storage as part of the solution. The technological barrier to large scale CCS arises from high energy penalty to scrubbing CO_2 with current methods. Although P/TSA systems are among the most energy efficient CO_2 scrubbing technologies, better sorbent materials are still needed. In this work, IISERP-MOF**2** was found to have the lowest PE reported for postcombustion CO_2 capture, outperforming even Mg-MOF-74 (655 vs 695 kJ/kg CO_2). **1** has a modest CO_2 uptake at 0.15 bar and 313 K, an exceptional CO_2:N_2 selectivity of 1853 and low heat of adsorption. In addition to the record low PE, **1** has remarkable hydrolytic stability, smooth separation kinetics as evidence from the dry and humid breakthrough measurements, easy scalability, and is made from readily available and inexpensive precursors, making it a highly promising candidate for large scale postcombustion CO_2 capture even under humid conditions. This work further

DOI: 10.1021/jacs.6b10455
J. Am. Chem. Soc. 2017, 139, 1734−1737

shows that ultramicroporous MOFs can be excellent materials for gas separation applications.

■ ASSOCIATED CONTENT

Supporting Information

The Supporting Information is available free of charge on the ACS Publications website at DOI: 10.1021/jacs.6b10455.

Materials and calculation methods (PDF)
Data for $C_{15}H_{15}N_3NiO_5$ (CIF)

■ AUTHOR INFORMATION

Corresponding Authors

*vaidhya@iiserpune.ac.in
*twoo@uottawa.ca
*Praveen.thallapally@pnnl.gov

ORCID

Sean Collins: 0000-0001-6153-8515
Ramanathan Vaidhyanathan: 0000-0003-4490-4397

Author Contributions

⊥These authors contributed equally.

Notes

The authors declare no competing financial interest.
CIF file available at Cambridge Crystallography Database. CCDC code: 1508166.

■ ACKNOWLEDGMENTS

We thank Dr. J.M. Huck for help in calculating the parasitic energies. We acknowledge IISER-Pune, NSERC of Canada, and the MHRD-FAST program for the necessary funding.

■ REFERENCES

(1) *CO_2 Emissions from Fuel Combustion Highlights*, 2015 ed.; OECD/IEA, 2015.
(2) Singh, D.; Croiset, E.; Douglas, P. L.; Douglas, M. A. *Energy Convers. Manage.* **2003**, *44*, 3073.
(3) (a) Huck, J. M.; Lin, L.-C.; Berger, A. H.; Shahrak, M. N.; Martin, R. L.; Bhown, A. S.; Haranczyk, M.; Reuter, K.; Smit, B. *Energy Environ. Sci.* **2014**, *7*, 4132. (b) Lin, L.-C.; Berger, A. H.; Martin, R. L.; Kim, J.; Swisher, J. A.; Jariwala, K.; Rycroft, C. H.; Bhown, A. S.; Deem, M. W.; Haranczyk, M.; Smit, B. *Nat. Mater.* **2012**, *11*, 633. (c) *CO_2 Capture from Existing Coal-Fired Power Plants*; DOE/NETL-401/110907; US DOE, South Park Township, 2007.
(4) Ciferno, J. P.; Fout, T. E.; Jones, A. P.; Murphy, J. T. *Chem. Eng. Prog.* **2009**, *105*, 33.
(5) Ko, D.; Siriwardane, R.; Biegler, L. T. *Ind. Eng. Chem. Res.* **2003**, *42*, 339.
(6) (a) Pirngruber, G. D.; Carlier, V.; Leinekugel-le-Cocq, D. *Oil Gas Sci. Technol.* **2014**, *69*, 989. (b) Joos, L.; Swisher, J. A.; Smit, B. *Langmuir* **2013**, *29*, 15936.
(7) (a) Li, J.-R.; Ma, Y.; McCarthy, M. C.; Sculley, J.; Yu, J.; Jeong, H.-K.; Balbuena, P. B.; Zhou, H.-C. *Coord. Chem. Rev.* **2011**, *255*, 1791. (b) Nguyen, N. T. T.; Furukawa, H.; Gandara, F.; Nguyen, H. T.; Cordova, K. E.; Yaghi, O. M. *Angew. Chem., Int. Ed.* **2014**, *53*, 10645. (c) Fracaroli, A. M.; Furukawa, H.; Suzuki, M.; Dodd, M.; Okajima, S.; Gándara, F.; Reimer, J. A.; Yaghi, O. M. *J. Am. Chem. Soc.* **2014**, *136*, 8863. (d) Zhou, H. -C. J.; Kitagawa, S. *Chem. Soc. Rev.* **2014**, *43*, 5415. (e) Xiang, S.; He, Y.; Zhang, Z.; Wu, H.; Zhou, W.; Krishna, R.; Chen, B. *Nat. Commun.* **2012**, *3*, 954. (f) Benson, O.; da Silva, I.; Argent, S. P.; Cabot, R.; Savage, M.; Godfrey, H. G. W.; Yan, Y.; Parker, S. F.; Manuel, P.; Lennox, M. J.; Mitra, T.; Easun, T. L.; Lewis, W.; Blake, A. J.; Besley, E.; Yang, S.; Schröder, M. *J. Am. Chem. Soc.* **2016**, *138*, 14828.
(8) (a) Bhatt, P. M.; Belmabkhout, Y.; Cadiau, A.; Adil, K.; Shekhah, O.; Shkurenko, A.; Barbour, L. J.; Eddaoudi, M. *J. Am. Chem. Soc.* **2016**, *138*, 9301. (b) Liao, P.-Q.; Chen, X.-W.; Liu, S.-Y.; Li, X.-Y.; Xu, Y.-T.; Tang, M.-N.; Rui, Z.-B.; Ji, H.-B.; Zhang, J.-P.; Chen, X.-M. *Chem. Sci.* **2016**, *7*, 6528. (c) Zhou, H. C. J.; Long, J. R.; Yaghi, O. M. *Chem. Rev.* **2012**, *112*, 673. (d) Bae, Y.-S.; Farha, O. K.; Hupp, J. T.; Snurr, R. Q. *J. Mater. Chem.* **2009**, *19*, 2131. (e) Zhang, Z.; Yao, Z.-Z.; Xiang, S.; Chen, B. *Energy Environ. Sci.* **2014**, *7*, 2868. (f) Vaidhyanathan, R.; Iremonger, S. S.; Shimizu, G. K. H.; Boyd, P. G.; Alavi, S.; Woo, T. K. *Science* **2010**, *330*, 650. (g) An, J.; Geib, S. J.; Rosi, N. L. *J. Am. Chem. Soc.* **2010**, *132*, 38. (h) Dzubak, A. L.; Lin, L.-C.; Kim, J.; Swisher, J. A.; Poloni, R.; Maximoff, S. N.; Smit, B.; Gagliardi, L. *Nat. Chem.* **2012**, *4*, 810. (i) Kumar, A.; Madden, D. G.; Lusi, M.; Chen, K.-J.; Daniels, E. A.; Curtin, T.; Perry, J. J., IV; Zaworotko, M. J. *Angew. Chem., Int. Ed.* **2015**, *54*, 14372.
(9) (a) Mason, J. A.; Sumida, K.; Herm, Z. R.; Krishna, R.; Long, J. R. *Energy Environ. Sci.* **2011**, *4*, 3030. (b) Furukawa, H.; Cordova, K. E.; O'Keeffe, M.; Yaghi, O. M. *Science* **2013**, *341*, 1230444.
(10) (a) Nandi, S.; De Luna, P.; Daff, T. D.; Rother, J.; Liu, M.; Buchanan, W.; Hawari, A. I.; Woo, T. K.; Vaidhyanathan, R. *Sci. Adv.* **2015**, *1*, e1500421. (b) Nandi, S.; Haldar, S.; Chakraborty, D.; Vaidhyanathan, R. *J. Mater. Chem. A* **2017**, *5*, 535.
(11) (a) Nugent, P.; Belmabkhout, Y.; Burd, S. D.; Cairns, A. J.; Luebke, R.; Forrest, K.; Pham, T.; Ma, S.; Space, B.; Wojtas, L.; Eddaoudi, M.; Zaworotko, M. J. *Nature* **2013**, *495*, 80. (b) Mason, J. A.; McDonald, T. M.; Bae, T. H.; Bachman, J. E.; Sumida, K.; Dutton, J. J.; Kaye, S. S.; Long, J. R. *J. Am. Chem. Soc.* **2015**, *137*, 4787.
(12) (a) Kizzie, A. C.; Wong-Foy, A. G.; Matzger, A. J. *Langmuir* **2011**, *27*, 6368. (b) Yu, J.; Balbuena, P. B. *J. Phys. Chem. C* **2013**, *117*, 3383.
(13) (a) Saha, D.; Bao, Z.; Jia, F.; Deng, S. *Environ. Sci. Technol.* **2010**, *44*, 1820. (b) Zhao, Z.; Li, Z.; Lin, Y. S. *Ind. Eng. Chem. Res.* **2009**, *48*, 10015.
(14) Silva, J. A. C.; Schumann, K.; Rodrigues, A. E. *Microporous Mesoporous Mater.* **2012**, *158*, 219.
(15) Elsaidi, S. K.; Mohamed, M. H.; Schaef, H. T.; Kumar, A.; Lusi, M.; Pham, T.; Forrest, K. A.; Space, B.; Xu, W.; Halder, G. J.; Liu, J.; Zaworotko, M. J.; Thallapally, P. K. *Chem. Commun.* **2015**, *51*, 15530.
(16) (a) Ye, Y.; Xiong, S.; Wu, X.; Zhang, L.; Li, Z.; Wang, L.; Ma, X.; Chen, Q. H.; Zhang, Z.; Xiang, S. *Inorg. Chem.* **2016**, *55*, 292. (b) Yao, Z.; Chen, Y.; Liu, L.; Wu, X.; Xiong, S.; Zhang, Z.; Xiang, S. *ChemPlusChem* **2016**, *81*, 850−856.

DOI: 10.1021/jacs.6b10455
J. Am. Chem. Soc. 2017, 139, 1734−1737